Phosphonate monolayers on InAsSb and GaSb surfaces for mid-IR plasmonics

Mario Bomers, Aude Mezy, Laurent Cerutti, Franziska Barho, Fernando Gonzalez-Posada, Eric Tournié, Thierry Taliercio

Phosphonate monolayers on InAsSb:Si and GaSb surfaces for mid-IR plasmonics

Mario Bomers,[1,*] Aude Mezy,[2] Laurent Cerutti,[1] Franziska Barho,[1] Fernando Gonzalez-Posada Flores,[1] Eric Tournié,[1] and Thierry Taliercio[1]

[1] *IES, Université de Montpellier, CNRS, Montpellier, France*
[2] *SiKÉMIA, F-34095 Montpellier, France*
**mario.bomers@umontpellier.fr*

Abstract: Stable functionalization of semiconductor surfaces is a prerequisite for all-semiconductor mid-IR biophotonics. This work demonstrates the adsorption of phosphonic acids on oxygen plasma activated GaSb and InAsSb surfaces. X-ray photoelectron spectroscopy shows that oxygen plasma treatment, used to activate the investigated III-V surfaces, increases the surface oxide layer beyond its native oxide thickness. Phosphonates with different terminal groups, either ethylene glycol or fluorinate carbon terminated groups, allow to modify the hydrophobicity of the surfaces and to protect the surfaces by an anti-fouling cover layer. Infrared spectroscopy indicates partial deprotonation of the phosphonic acid and thus phosphonate bonding to the surfaces. Adsorption of phosphonates on an all-semiconductor mid-IR plasmonic grating structure is detected by a shift and by a shape modulation of the plasmonic resonance peak. Compared with molecule adsorption on flat mirror-like layers a ten-fold signal enhancement is found. The adsorbed molecules are stable upon baking at 120° C, ultrasonic cleaning with organic solvents and storage for several weeks at ambient conditions. These results show that stable functionalization of InAsSb and GaSb surfaces by phosphonate monolayers is possible. All-semiconductor enhanced plasmonic sensing in the mid-IR was demonstrated.

1. INTRODUCTION

Mid-IR biophotonics at the interface of photonics and biomedical science requires light sources, detectors and transducer elements. InAsSb and GaSb as narrow bandgap III-V materials are established materials for mid-IR sources and detectors [1]. Transducer elements, like subwavelength plasmonic gratings, allow surface-enhanced infrared spectroscopy [2]. Instead of CMOS – incompatible transducers based on gold, an all-semiconductor approach with potential on-chip integration is favorable. It could be shown that gratings made from highly Si-doped InAsSb grown lattice matched on GaSb allows to excite localized surface plasmon resonances (LSPR) in the range from 5-15 µm [3].

A major challenge of highly-doped semiconductor as alternative plasmonic material [4,5] is the functionalization of the surface [6]. Thermodynamic stability of the semiconductor surface and stable bonding of molecules to the semiconductor surface are prerequisites for biomolecular interfaces [7].

The chemistry of the interfaces of GaSb, InAs and the derivative InAsSb are well studied [8]. At ambient conditions, native oxides form layers in the order of few nanometer on the surface. In a long-time air oxidation study, it could be shown that a 3 nm thick native oxide layer appears on GaSb within one day whereas after 3 years this layer increases only moderately by 1 nm [9]. The hydrolytic stability for InAs in neutral water was reported [10], but GaSb oxidizes in an aqueous environment [11,12].

As the optoelectronic properties of GaAs, GaSb and InAs are depending on passivated surfaces, a promising approach consists in etching the native oxide layer and forming metal-thiol bonds [13–15]. Despite successful monolayer formation, the III-V surfaces passivated by thiol bonding are not stable upon reoxidation at ambient conditions [16,17]. Nevertheless, it could be demonstrated that the thiols bond on InAs decreases indium and arsenic leaching under physiological condition [10]. To prevent reoxidation, a potential solution could be the formation of thicker organic layer e.g. by diazonium chemistry [18,19].

In this work we present an alternative approach by working with the native oxide instead of against it. For GaAs, it could be shown that phosphonic acid ligands not only bind to the surface, but they give as well a higher monolayer coverage than thiol bond ligands [20]. This confirms earlier works on GaAs where biomolecule coupling to GaAs via phosphonate bonding was demonstrated [21]. Another study of phosphonic acid adsorption on GaAs demonstrates that while a water-free solvent during phosphonic acid adsorption leads to monolayer formation, a water content > 4% leads to multiple physiosorbed layers [22].

To our knowledge there are no studies on phosphonic acid adsorption on GaSb and InAsSb surfaces, but the results for phosphonic acid adsorption on GaAs and the existence of a native oxide layer on these materials motivate

a functionalization approach based on working with the native oxide by phosphonate bonding instead of working against the oxidation by thiol bonding. In a review of covalent surface modification of oxide surfaces [23] the authors write that the reactivity of oxide surfaces depends mainly on the surface OH-groups. An increase in reactivity can be obtained by activation of these groups by e.g. etching or plasma treatment. According to the authors of [23], the phosphonic acid reaction offers the advantage of (1) relative easy synthesis and purification, (2) absence of homo-condensation and (3) a good hydrolytic stability. In a review dedicated to phosphonate coupling [24], the term phosphonate signifies the mono-deprotonated $RPO_2(OH)^-$ and the fully deprotonated RPO_3^{2-} form of the phosphonic acid. The authors describe the coupling of phosphonic acids to oxide surfaces by the formation of ionocovalent P-O-M bonds by condensation of P-OH groups with surface M–OH groups. Up to three P-O-M bonds are possible and additionally hydrogen bonds between residual P-OH or P=O groups participate in the anchoring. Monodentate, bridging bidentate, bridging tridentate, chelating bidentate, chelating tridentate, and additional hydrogen-bonding interactions are possible bonding configurations [23]. Generally, the conformational order of alkyl phosphonic acids (PA) increases with chain length and decreases with temperature. For silane and phosphonate monolayers an increase of transition temperature from an ordered to a disordered state with increasing chain length was demonstrated [25,26]. Additionally, it was shown that the grafting stability of phosphonate monolayers increases for samples treated by an annealing step at 100°-150° C [20] and it was shown that the monolayers return to an ordered state after thermal disordering [26].

In this work, we investigate the phosphonic acid adsorption on InAsSb and GaSb surfaces. Highly mid-IR reflective samples have been fabricated by molecular beam epitaxy. A subwavelength mid-IR grating from the highly doped semiconductor material system allows to study plasmonic enhanced detection of phosphonate adsorption on semiconductor surfaces. The successful surface modification of these III-V surfaces was demonstrated by two different phosphonate functional groups, (1) by a hydrophobic fluorinated end group and (2) by an anti-fouling methoxy terminated ethylene glycol group.

2. MATERIALS AND METHODS

2.1 Mid-IR reflective layer structures and plasmonic grating fabrication

The adsorption experiments were performed on two types of surface, InAsSb and GaSb. The III-V semiconductor layer structures are grown on Te-doped (001) GaSb substrates by solid-source molecular beam epitaxy (MBE). After thermal de-oxidation of the wafer, a 300 nm thick non-intentionally doped GaSb buffer was grown, followed by a 1 µm thick Si-doped $InAs_{0.9}Sb_{0.1}$ layer. This is the InAsSb-surface sample that we have investigated. A doping level of $5x10^{19}$ cm^{-3} corresponding to a plasma wavelength of 5.5 µm was determined for the $InAs_{0.9}Sb_{0.1}$ layer [27]. The highly-doped $InAs_{0.9}Sb_{0.1}$-layer acts as a mirror-layer for wavelengths above the plasma wavelength. To investigate adsorption experiments on a GaSb-surface, a 50 nm GaSb top-layer is added to the 1 µm thick Si-doped $InAs_{0.9}Sb_{0.1}$ layer, subsequently named the GaSb-surface sample.

For the plasmonic grating, a 100 nm thick Si-doped $InAs_{0.9}Sb_{0.1}$ layer was grown on a Te-doped (001) GaSb substrate and holography was used to define a stripe pattern using AZMIR 701 positive photoresist. Dry etching was used to obtain InAsSb-ribbons of 100 nm (± 2 nm) height, 325 nm (± 20 nm) width and a grating period of 450 nm (± 5 nm). Details on the fabrication can be found in previous work [3,28].

2.2 Chemical products and surface modification

12,12,13,13,14,14,15,15,16,16,17,17,18,18,19,19,19-Heptadecafluorononadecylphosphonic acid (Cas N. 625095-76-3) and (6-{2-[2-(2-Methoxy-ethoxy)-ethoxy]-ethoxy}-hexyl)phosphonic acid (Cas N. 1049677-18-0) were synthesized by Sikemia. For the sake of simplicity, in the following, we will call the phosphonic acid with the fluorinated terminate group FDPA and the phosphonic acid with the methoxy-terminated ethylene glycol group EGPA. Ethanol (API, > 99 %) and chloroform (Carlo Erba reagents, > 99 %) were used as received. The wafer with the InAsSb-surface, the wafer with the GaSb-surface, and the plasmonic grating were cleaved into 10 mm x 10 mm pieces.

The adsorption experiment started with dissolving the FDPA, respectively the EGPA, in 10 ml of ethanol to obtain 1 mM solutions. To rinse the surfaces from contaminations, the cleaved III-V samples were sonicated for 3 min in ethanol and then for 3 min in chloroform. Then, we have tested two different experimental protocols to discuss the role of plasma surface activation and reaction time on the adsorption of phosphonates. Process I consists in exposing the III-V surfaces for 40 s to O_2-plasma at 100 W and 20 mbar (PicoPCCE, Diener electronics) and then to immerse the samples in 10 ml of the 1 mM solutions for 6 h. Process II consists in a softer O_2-plasma treatment (100 W, 0.5 mbar, 10 s) and a longer immersion time of 48 h. After the immersion, all samples were baked for 12 h

in an oven at 120 °C (UF260, Memmert) to increase the grafting stability. To investigate the influence of the plasma and the solvent, we immersed a sample per surface type (InAsSb, respectively GaSb) after the plasma treatment and before the baking in 10 ml of pure ethanol, subsequently called dummy process. Finally, all samples were rinsed by ethanol and sonicated for 3 min in ethanol and for 3 min in chloroform.

The grating surfaces were modified according to process II, where the milder O_2-plasma treatment is expected to guarantee surface activation, but to increase only moderately the amount of surface oxides. We compare a dummy treated grating (pure ethanol immersion), a FDPA treated surface (1 mM FDPA immersion) and an EGPA treated surface (1 mM EGPA immersion). As for the III-V layer samples, the gratings were rinsed and sonicated after the baking step and before the subsequent characterization steps.

2.3 Characterization techniques

To determine the hydrophobic properties of the surface after the different treatment, water contact angles were measured 6 h after sonication by the Digidrop Fast/60 model. The measurements were performed at room temperature under ambient conditions where nominal 2.5 µl of de-ionized water was dispersed from a micro-burette and an image was taken 100 ms after drop deposition. To avoid oxidation of the III-V surface through the water drop, the surfaces were rinsed with ethanol and then with chloroform after the images were taken. After three month of storage at ambient conditions the contact angle measurements were repeated to address long-time stability of the molecule adsorption.

X-ray photoelectron (XPS) spectra were measured by the Escalab 250 Thermo Electron system after storing the samples for 4 weeks at environmental conditions. Samples treated according to process I were investigated as stronger modification of the samples was expected for this process due to the harsher oxygen plasma conditions. The spot area of the Al Kα source (1486 eV) was 400 µm and the energy steps of the hemispherical analyzer in the constant analyzer energy (CAE) mode were 0.1 eV. The pass energy was set at 20.0 eV and the number of scans was varied for the detailed spectra: In 3d (5 scans), As 3d (30 scans), Sb 3d (5 scans), Ga 3d (20 scans) and C 1s (20 scans).

Fourier transform infrared (FTIR) reflection absorption spectroscopy was performed with a Hyperion 3000 IR microscope coupled to a Vertex 70 Fourier-transform IR spectrometer. The plasmonic gratings were investigated with the microscope x15 magnification Cassegrain objective (NA = 0.4) where light originating from a globar source was focused onto an imaging area of 100x100 µm^2. A polarizer in the beam path enabled polarization dependent detection of the reflection signal with a single element mercury cadmium telluride detector. The flat surfaces were measured by the ATR module of the microscope which consists of an x20 objective which couples incident light with angles from 10°-24° into a Ge-waveguide crystal to a 32x32 µm^2 imaging area. Non-polarized light was used in this configuration.

The geometry of the plasmonic grating was characterized with a Fei Inspect S-50 scanning electron microscope (SEM) at an electron-beam energy of 20 kV.

3. RESULTS AND DISCUSSION

3.1 Contact Angle Measurements

In Figure 1, the modification process I (40 s plasma, 6 h immersion time) is sketched and the results of the contact angle measurements on the InAsSb:Si surfaces are shown. It can be seen that the water drop brought to contact with the FDPA treated surface did only partly detach from the micro-burette. Such a partial detachment was neither observed for the other surfaces, nor for the FDPA surface after 3 months of storage. The contact angle was determined by the $\theta/2$ – method from the image taken 100 ms after drop deposition [29]. After 3 months of storage under ambient conditions the contact angle measurements were repeated and the results are summarized in Table 1.

Table 1: Contact angle measurements of III-V surfaces treated by process I. Values are reported for surfaces modified by phosphonic acid with hydrophobic (FDPA) and hydrophilic (EGPA) terminated groups, for surfaces modified by O_2-plasma and ethanol treatment (dummy) and for non-treated reference surfaces immediately after the surface treatment (t_0) and three month later.

	FDPA	EGPA	Dummy	Reference
GaSb – surface (t_0)	100° (± 10°)	54° (± 2°)	66° (± 2°)	-
(t_0 + 3 months)	100° (± 2°)	68° (± 2°)	80° (± 2°)	90° (± 2°)
InAsSb – surface (t_0)	101° (± 10°)	57° (± 2°)	70° (± 2°)	-
(t_0 + 3 months)	106° (± 2°)	65° (± 2°)	92° (± 2°)	94° (± 2°)

The GaSb and the InAsSb surfaces with FDPA are more hydrophobic, i.e. they have larger contact angles than the dummy surfaces. The only partial detachment of the drop leads to smaller amount of water on these surfaces and the resulting reduction of imaging contrast leads to a relative large error interval. In the literature, a contact angle of 101° (± 1°) was reported for Indium-Tin Oxide surfaces treated with a comparable fluorinated phosphonic acid [30]. This value is in good agreement with the values we measured on GaSb and InAsSb surfaces.

The surfaces treated with EGPA are less hydrophobic, so smaller contact angles than for the dummy surfaces were found. In the literature, a contact angle of 63° (± 2°) was reported for surfaces modified with a methodoxy-terminated tri(ethylene glycol) end group, i.e. an end group comparable to the used EGPA molecules [31]. The authors discuss differences in contact angle in terms of disorder of the layer and of ether oxygen accessible to the liquid. We limit our discussion to the observation that 6 h after completing process I, the FDPA treated surfaces are more hydrophobic than the dummy surfaces and the EGPA surfaces are more hydrophilic than the dummy surfaces.

After 3 months of storage, the contact angle of the dummy surface and the reference sample are very similar. The contact angle values are significantly higher than those obtained 6 h after the modification experiment. We explain this harmonization by an increase of surface contamination due to exposure to the environment. The surfaces treated by FDPA (resp. EDPA) are, even after 3 months, more (resp. less) hydrophobic than the dummy and the reference samples. This hints that the molecular-treatment passivates the surface. We conclude that the phosphonic acids adsorbed according to process I (1) modify the surface properties, (2) remain adsorbed when sonicated in ethanol and chloroform and, (3) remain adsorbed when the surface is exposed to environmental conditions.

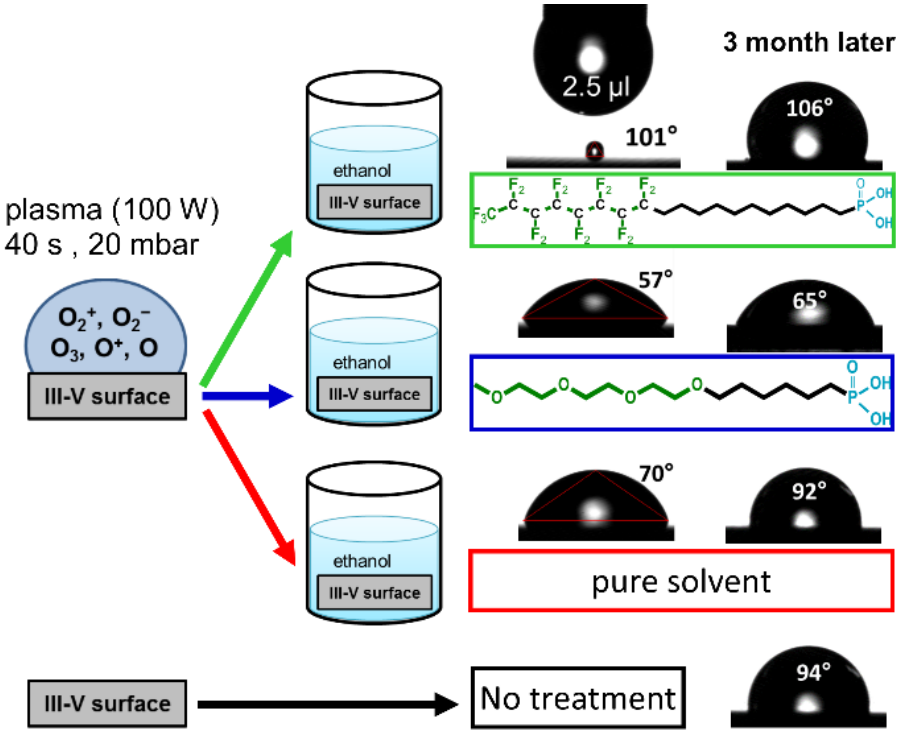

Figure 1: The modification process I (40 s plasma, 6 h immersion time) is sketched and the contact angle measurements with deionized water were measured after the III-V samples were baked, sonicated for 3 min in organic solvents, blown dry by inert N_2 gas and stored at ambient conditions for 6 h. After 3 months of storage the measurements were repeated.

Additional to the contact angle measurements, we have performed ellipsometry and atomic force microscopy (AFM) measurements before and after treatment by process I and process II (not shown). As the ellipsometry technique is sensitive to detect nanoscale modifications of reflective layer-structures, we used this to confirm that the dummy treatment, as well as the molecule treatment, modifies the optical response. Especially for the InAsSb-surfaces, the dummy treatment of process I led to a more pronounced modification than process II. By mapping the surface morphology with an atomic force microscope we found that the dummy treatment is not increasing the roughness of the native oxide layer, contrary to the molecule deposition (EGPA adsorption) which was increasing the roughness by a factor of two (from root mean squared roughness of 0.26 nm to 0.55 nm), respectively by a factor of four (FPDA adsorption). The ellipsometry and the AFM approach did not allow to distinguish between an additional

oxide layer and an additional molecular layer, so we decided to address the hypothesis of a plasma grown oxide layer by XPS-spectroscopy and to discuss differences in terms of molecular absorption due to process I or process II by IR-spectroscopy.

3.2 X-ray photoelectron spectroscopy

The atomistic changes at the surfaces due to process I were investigated by X-ray photoelectron spectroscopy 4 weeks after the samples were baked, sonicated and stored at ambient conditions. For each material surface, InAsSb or GaSb, a reference sample which received no treatment according to process I was characterized together with the FDPA, the EGPA and the dummy treated samples (see Figure 1 for illustration). The analyzer resolution of the spectrometer is ± 0.2 eV and for the sake of readability, we neglect a detailed error discussion in the following.

In Figure 2, the survey scans of the modified InAsSb and GaSb surfaces are shown. The spectra are dominated by signatures originating from the III-V elements, but the fluorine F (1s) peak, only present for the surfaces treated by FDPA, demonstrates clearly the adsorption of the molecule. As the antimony Sb ($3d_{5/2}$) peak is overlapping with the oxygen O (1s) peak, we first deconvoluted the Sb ($3d_{3/2}$) peak and then we used the fixed ratio between the Sb ($3d_{3/2}$) and the Sb ($3d_{5/2}$) peak to deconvolute the oxygen peak. In Table 2 the determined surface element concentrations are summarized. We find that the dummy process increases the amount of oxygen (compared to the reference surface). The presence of phosphorous indicates clearly the phosphonic acid adsorption.

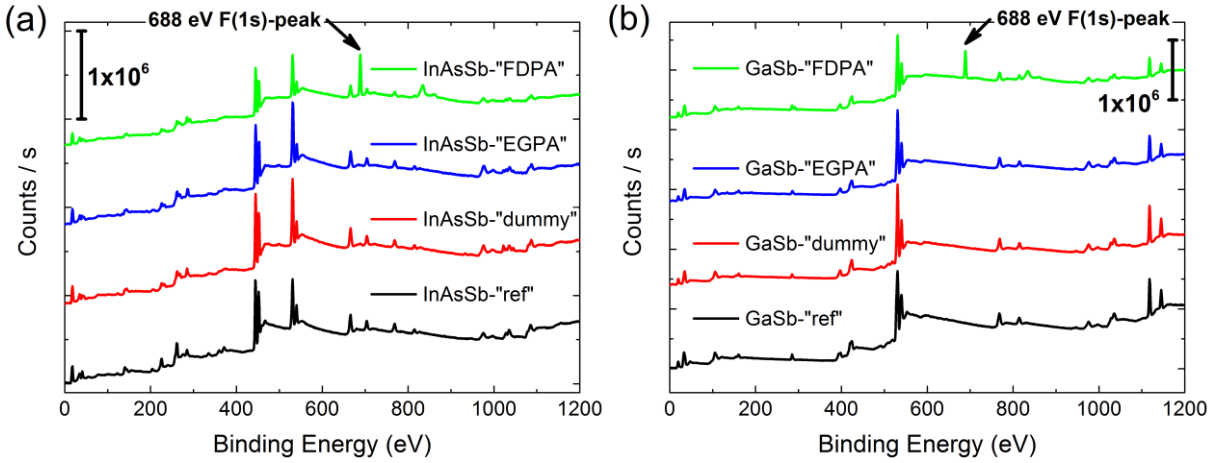

Figure 2: X-ray photoelectron spectroscopy on (a) InAsSb-surfaces and (b) GaSb-surfaces stored at ambient conditions for 4 weeks after completion of the grafting process.

Table 2: Surface elements concentration in percent for the InAsSb and GaSb surfaces treated by process I.

		"FDPA"	"EGPA"	"dummy"	"ref"
InAsSb	In (3d)	7.9	10.5	12.7	17.1
	As (3d)	7.4	10.9	11.5	15.4
	Sb (3d)	2.6	4.1	4.4	6.2
	O (1s)	29.6	50.1	48.2	38.4
	C (1s)	26.7	21.9	23.2	22.9
	P (2p)	1.1	2.5	-	-
	F (1s)	24.7	-	-	-
GaSb	Ga (2p)	8.0	12.4	16.9	18.8
	Sb (3d)	8.1	10.6	12.2	14.1
	O (1s)	38.3	56.3	55.1	45.2
	C (1s)	21.9	17.7	15.8	21.9
	P (2p)	1.7	3.0	-	-
	F (1s)	22.0	-	-	-

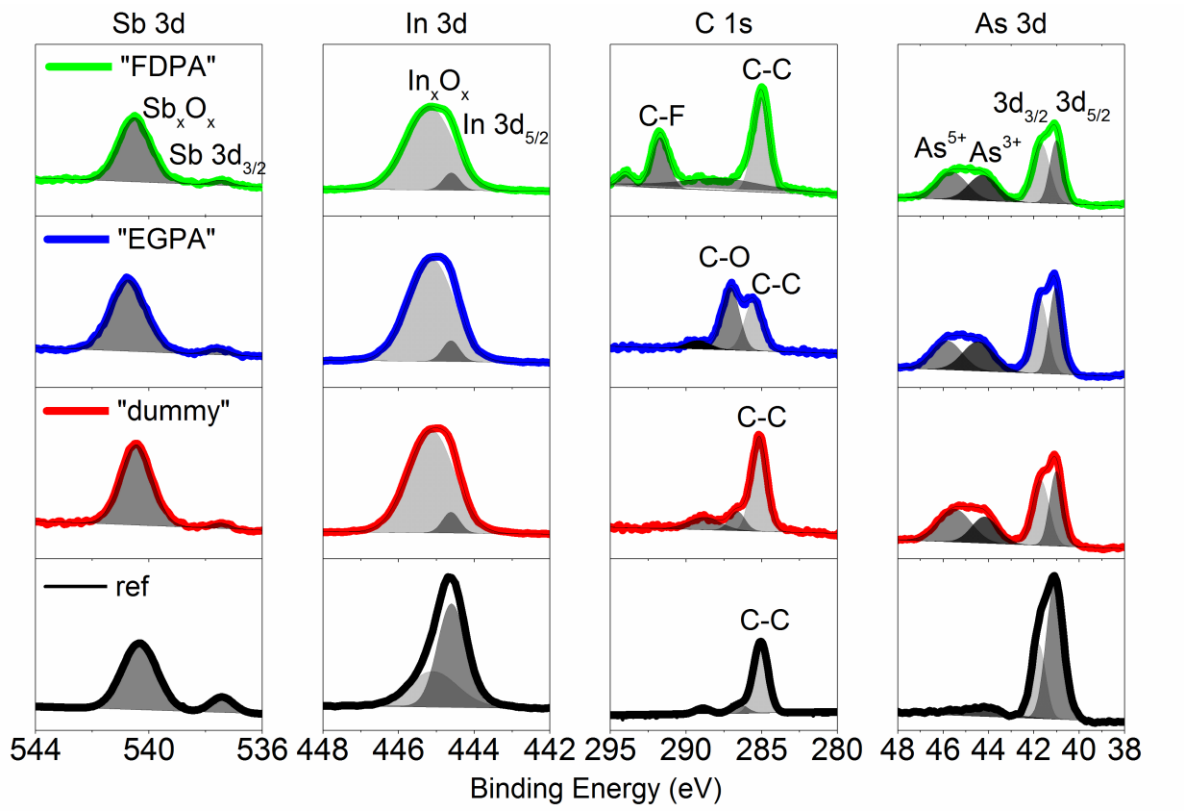

Figure 3: X-ray photoelectron spectroscopy on InAsSb-surfaces stored at ambient conditions for 4 weeks after completion of the grafting process. The detailed spectra of Sb 3d, In 3d, C 1s and As 3d indicate a clear increase of surface oxide components and significant spectral signatures of the respectively adsorbed molecules as explained in the text.

More information on the oxidation and the grafting process can be obtained by focusing on selected spectral regions. In Figure 3, the results for the InAsSb-surfaces are shown. The detailed spectra of Sb 3d, In 3d, C 1s and As 3d indicate a clear increase of surface oxide components and significant spectral signatures of the respectively adsorbed molecules as will be explained in the following. The peaks were deconvoluted by assuming Gaussian peaks contrasting from the background. The deconvolution of the Sb $3d_{3/2}$ signature reveals two peaks. The dominant peak centered at 540.5 eV can be attributed to Sb-O bonding and the weaker peak centered at 537.4 eV to Sb-In bonding [23]. The In 3d spectra can be deconvoluted by a weak peak at 444.6 eV and a dominant peak at 445.1 eV. In the compound $InAs_{0.9}Sb_{0.1}$, Indium can form bonds with As, Sb and O. XPS-spectra of InAs and InSb [14,16,32] allow to attribute the peak at 445.1 eV to an In^{3+} (In_2O_3) state and the weaker peak at 444.6 eV to In-As, respectively to In-Sb bonding. The As $3d_{5/2}$ spectra could be deconvoluted by four peaks with maxima at 41.0 eV, 41.7 eV, 44.2 eV and at 45.2 eV. A comparison with literature values allows to attribute the peaks lowest in binding energy to the spin-orbit components (Δ=0.7 eV) of the InAs bond and to attribute the two peaks at higher binding energy to oxidation states [33], i.e. a As^{3+} and a As^{5+} state. The detailed C 1s spectra indicate clearly the presences of the molecules FDPA and EGPA on the surfaces of the respectively treated samples. While adventitious carbon (C-C at 284.8 eV, C-O-C at ~286 eV and O-C=O at ~288.5 eV) could be measured on all samples, a peak at 291.7 eV corresponding to the $(CF_2)_7$ terminate group and a peak at 294.0 eV corresponding to the CF_3 terminus were measured only on the FDPA treated sample [30]. The C 1s spectra of the surface modified by EGPA can be deconvoluted by two similarly strong peaks centered at 285.5 eV and at 287.1 eV. We attribute the first peak to the alkyl groups of EGPA and to adventitious carbon and the second peak can be attributed to ether carbon atoms [31].

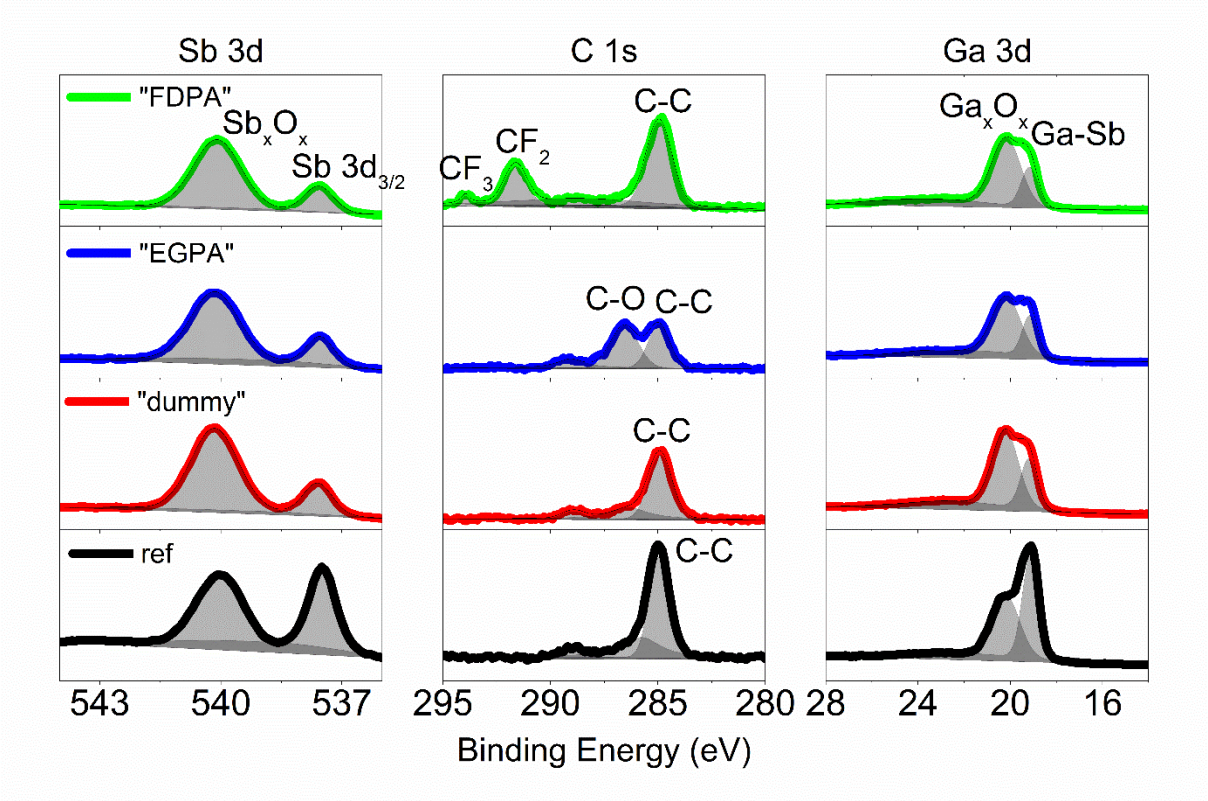

Figure 4: X-ray photoelectron spectroscopy on GaSb-surfaces stored at ambient conditions for 4 weeks after completion of the grafting process. The detailed spectra of Sb 3d, C 1s and Ga 3d indicate a clear increase of surface oxide components and significant spectral signatures of the respectively adsorbed molecules as explained in the text.

In Figure 4, the results for the GaSb-surface are shown. The detailed spectra of Sb 3d, C 1s and Ga 3d indicate a clear increase of surface oxide components and significant spectral signatures of the respectively adsorbed molecules. The deconvolution of the Sb $3d_{3/2}$ signature reveals two peaks. The dominant peak centered at 540.1 eV can be attributed to Sb-O bonding and the weaker peak centered at 537.5 eV to Sb-Ga bonding [32]. The Ga 3d spectra can be deconvoluted by two peaks and we attribute the peak at 20.2 eV to Ga-Sb bonding and the peak at 19.2 eV to Ga-O bonding [32]. The deconvolution of the C 1s spectra of the GaSb-surfaces is identical to the spectra obtained on the InAsSb-surfaces.

The deconvolution of the X-ray photoelectron spectra allows to determine peak area ratios which are summarized in Table 3. For the InAsSb surface and the GaSb surface, we find a significant modification of the peak area ratio for In, As, Sb, Ga and their respective oxide states for the surfaces treated by process I compared to the reference sample. The differences in peak area ratio for the surfaces treated by different molecules is negligible and we conclude that it is very likely that the plasma treatment is causing the significant increase of the oxide components.

The deconvolution of the C 1s is not only clearly indicating the presence of FDPA and EGPA on the surfaces of the respectively treated samples, but the deconvolution allows as well to compare peak area ratios with stoichiometric ratios. The FDPA molecule with one CF_3 terminus and with seven fluorinated carbon atoms $(CF_2)_7$ gives a stoichiometric ratio of 0.14 (1/7). The determined peak area ratio of the CF_3 peak to the $(CF_2)_7$ peak is 0.19 on the InAsSb-surface (0.15 on the GaSb-surface). This value is higher than the stoichiometric ratio which indicates that the $(CF_2)_7$ chain is partly shielded by the CF_3 terminus, thus a weak ordering of the adsorbed molecules [34].

For the sample treated with EGPA, we find a peak area ratio of 1.22 between the polyether carbon peak and the peak attributed to alkyl and adventitious carbon. The value is close to the stoichiometric ratio of 1.4 (7/5) which hints hindering of adventitious carbon adsorption, thus anti-fouling properties.

Table 3: Peak area ratios indicating the plasma induced increase of surface oxides and the presence the FDPA and the EGPA molecule on the surface.

			"FDPA"	"EGPA"	"dummy"	"ref"
InAsSb	Sb 3d	(Sb-In) / (Sb-O)	0.05	0.06	0.04	0.15
	In 3d	(In-[As/Sb]) / (In^{3+})	0.07	0.07	0.07	1.69
	As 3d	(As-In) / (As^{3+})	2.58	2.52	3.03	7.68
	C 1s	(CF_3) / $(CF_2)_7$	0.19	-	-	-
		(C-O) / (C-C)	-	1.23	-	-
GaSb	Sb 3d	(Sb-Ga) / (Sb-O)	0.23	0.22	0.23	0.74
	Ga 3d	(Ga-Sb) / (Ga-O)	0.34	0.38	0.42	1.03
	C 1s	(CF_3) / $(CF_2)_7$	0.15	-	-	-
		(C-O) / (C-C)	-	1.22	-	-

We conclude that process I and in particular the plasma treatment does not only activate the surface, but increases permanently the amount of oxides on the surface. This increase of oxide is strongest for Indium, but as well marked for Arsenide, for Gallium, and for Antimony. The X-ray photoelectron spectra demonstrate clearly the adsorption of the phosphonic acids with different functional groups on InAsSb and GaSb surfaces.

3.3 Infrared spectroscopy on reflective layer structures

The contact angle measurements and the XPS-spectra demonstrate phosphonate adsorption on the investigated III-V surfaces modified by process I. Infrared spectra of molecule adsorption on MBE-grown reflective surfaces allow to discuss the bonding configuration and to obtain a reference IR-spectra for molecule adsorption on mid-IR plasmonic gratings fabricated from the same materials. The highly Si-doped 1 µm thick InAsSb-layer with its plasma wavelength λ_{plasma} at 5.5 µm is a mid-IR mirror as can be seen in Figure 5. The used ATR-microscopy configuration consists of a non-polarized light cone, described by an incidence angle θ_{in} between 10°-24°, guided through a hemispherical top-surface into a Germanium-waveguide crystal with a flat bottom surface in contact with the III-V surface by exerting a slight pressure. As the critical angle for the Ge-air interface is 14°, we used the crystal pending in air to normalize the reflectance measured for the Ge-crystal brought into contact with the III-V surface.

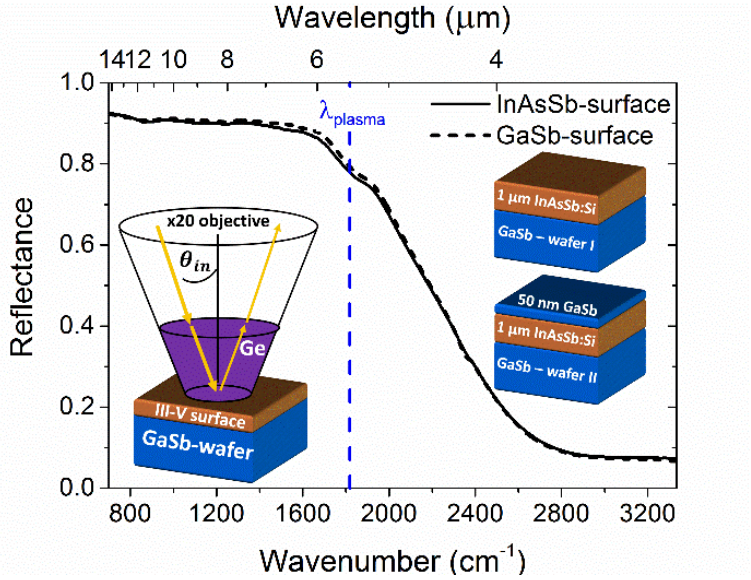

Figure 5: The solid line shows reflectance of highly-doped semiconductor InAsSb-surface and the dashed line shows the reflectance of a GaSb-surface. The illustrations sketch the measurement configuration and the investigated layer structures.

The solid line in Figure 5 shows the reflectance obtained for the reference InAsSb-surface and the dashed line shows the reflectance for the reference GaSb-surface. Despite a constant N_2-flow through the spectrometer, we limit the following discussion of IR-spectra on the atmospheric transmission window between 8 and 13 µm to avoid miss-assignment of peaks due to atmospheric fluctuations.

The IR-spectra were obtained one week after completion of process I and storage at ambient conditions. Additionally, IR-spectra were obtained for surfaces modified by the process II (softer plasma, longer immersion in solution). Two different material surfaces, two different processes and three different molecular solutions (FDPA, EGPA, dummy) yielded in total 12 different spectra. To obtain information about molecular vibration modes, we determined the ratio of the reflectance of a material surface with molecules $R_{molecule}$ and the reflectance of their respective dummy samples R_D. By subtracting unity, i.e. by plotting $(R_{molecule} - R_D)/R_D$ no significant difference in terms of molecular signatures according to process I and process II were found. Therefore, we take the average value of process I and process II to obtain one spectra per molecule and per material surface (4 spectra).

This data-treatment procedure, i.e. the normalization by the dummy spectra is optimized to reveal differences coming from the molecule attachment and not to reveal differences originating from differently strong plasma treatment, e.g. detection of oxide vibration modes. We chose this approach to demonstrate that despite having an influence on the oxide thickness, the plasma treatment and the immersion time (6 h or 48 h) has no influence on the molecular vibration spectra. Regarding the demonstrated increase of oxide XPS-signatures due to process I, we consider process II to be advantageous as the milder plasma did not lead to differences in the molecule IR-spectra and the weaker modification of the surface measured by ellipsometry (not shown) allows to assume that process II leads to a thinner oxide layer with the same amount of adsorbed molecules.

Additionally to the surface spectra, we show the bulk spectra of the respective molecules that were obtained with the same ATR-setup by depositing the powder (FDPA), respectively the liquid (EGPA), on a KBr-crystal. The measurement results are shown in Figure 6. One can clearly see that the surface spectral signatures are much weaker than those of the bulk spectra. To obtain a reference IR-spectra for comparison with molecule absorption on mid-IR plasmonic gratings consisting of InAsSb ribbons on GaSb we take the average value of molecule adsorption spectra on InAsSb surfaces (colored dashed line) and on GaSb surfaces (colored solid line) as being representative for the molecule absorption on these III-V surfaces (black solid line).

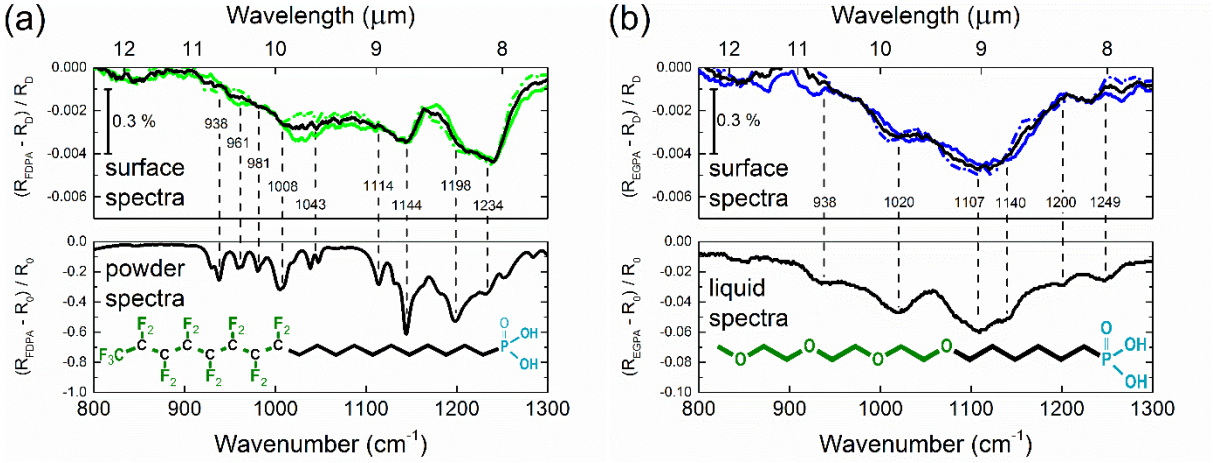

Figure 6 : (a) The spectra of the FDPA treated surface (top) is compared with its bulk powder spectra (bottom). (b) The spectra of the EGPA treated surface (top) is compared with its bulk liquid spectra (bottom). In the inset, a representation of the molecule is shown. The vertical dashed lines indicate spectral positions of interest. The colored dashed lines are the spectra for either the InAsSb or the GaSb surface. The black solid line is the average value of the spectra obtained on InAsSb and GaSb surfaces.

In Figure 6(a) the spectra of the FDPA treated surfaces is compared with its bulk spectra. It can be seen that the IR-peaks appear much sharper in the bulk spectra than in the surface spectra. Additionally, it can be seen that a spectral signature at 938 cm^{-1}, clearly visible in the bulk spectra, is not pronounced in the surface spectra. On the contrary, we can see that around 1043 cm^{-1} a broad absorption signature appears in the surface spectra. In a detailed study about phosphonic acid adsorption on GaAs [22], the authors investigate the role of the water content in the solvent for phosphonic acid adsorption on this III-V surface. They found that an anhydrous solution favors the formation of a low-density monolayer. They assigned the bands between 920-950 cm^{-1} to P-OH vibration modes and the peaks in between 970-1125 cm^{-1} to P-O stretching modes in hydrogenophosphonate or phosphonate ions. Following their line of argumentation, we suggest that the surface spectra shown in Figure 6(a) can be interpreted as a Langmuir-type adsorption where molecules are associated through hydrogen bonding (see non-vanishing P-OH

vibration) and ionocovelent bonding (IR-absorption in between 970-1125 cm^{-1}). The carbon-fluorine vibrations in between 1200-1250 cm^{-1}, representative for the FDPA molecule [35], allow a clear distinction from the surfaces modified by EGPA shown in Figure 6(b).

The EGPA spectrum is dominated by a strong peak around 1107 cm^{-1} assigned to C-O-C stretching vibrations [31]. As for the FDPA surface spectra, we can observe a weakening of the P-OH peak and an absorption feature in the spectral region attributed to hydrogenophosphonate or phosphante ion vibration modes. The differences between surface and bulk spectra are less marked for EGPA than for FDPA. While the FDPA bulk spectrum has sharp vibration features, the EGPA bulk spectrum is broadened. We explain this by the state-of-matter at room temperature: FDPA is a powder and EGPA is a viscous liquid at room temperature.

From the comparison of bulk and surface spectra, we can observe that (1) the functional groups (C-O-C, respectively C-F_2) allow a clear distinction of the differently treated surfaces, (2) vibration features appear broadened on the surface and (3) vibration modes in the P-OH range appear weakened, while absorption in the hydrogenophosphonate or phosphonate ion range is pronounced for the surface spectra. The absence of water in the solvent during the adsorption process and the sonication step after baking of the samples at 120° C indicate a low-density phosphonate monolayer.

3.4 Mid-IR plasmonic sensing of phosphonate adsorption

To demonstrate plasmonic enhanced sensing of phosphonate adsorption on III-V surfaces, we used a grating of InAsSb ribbons on a GaSb substrate. Figure 7(a) illustrates the fabrication process of the plasmonic grating. It can be seen that the layer structure before nanostructuration by photolithography and etching is comparable with the previously studied flat-layer structures. To guarantee surface activation, but minimize surface oxidation, we choose the parameters of process II due to its milder plasma treatment for this experiment.

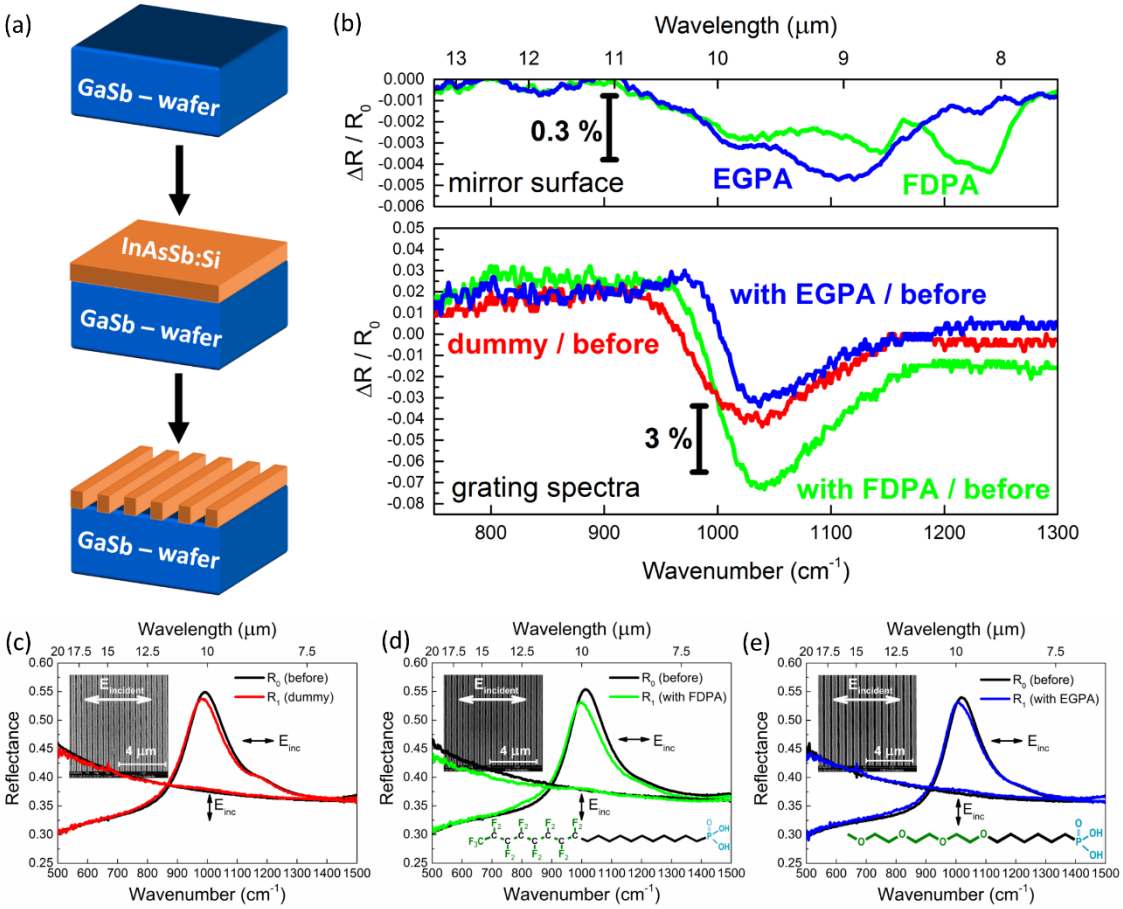

Figure 7 : (a) A sketch of the grating fabrication process. (b) On top, the reference spectra of FDPA and EGPA on mirror surfaces are shown. On the bottom, the ratio before/after treatment is shown for the dummy treated grating (solid red curve),

the FDPA treated grating (green curve) and the EGPA treated grating (blue curve). (c) The reflectance of the grating before (black solid lines) and after the dummy treatment (red solid line) is shown for light polarized parallel and perpendicular to the ribbons. In the inset, a scanning electron image of the surface before treatment is shown. (d) The reflectance of the grating before (black solid lines), after FDPA treatment (green solid line) and a representation of the molecule are shown. (e) The reflectance of the grating before (black solid lines) and after EGPA treatment (blue solid line).

In Figure 7(b) the IR-spectra obtained on flat mirror-like surface (top spectra) are compared with the spectra of mid-IR plasmonic gratings modified by phosphonic acid adsorption (bottom spectra). The modulation of the grating reflectance upon surface modification is shown in Figure 7(c-e). Scanning electron images are added in the inset to illustrate successful grating fabrication. In Figure 7(c) the modification of the grating which received the dummy treatment (O_2-plasma, immersion in ethanol and sonication in organic solvents) is shown. The reflectance measurements were obtained in the FTIR-microscope configuration with an imaging area of 100x100 μm^2 and quasi-normal incident light. Only for incident light polarized perpendicularly to the grating a plasmonic reflectance peak is observable. This allows to attribute the strong reflectance peak to a localized surface plasmon resonance (LSPR) mode centered at 10 µm. The dummy treatment modifies the plasmonic resonance. Compared with the reflectance before the treatment (black solid line), the reflectance after the treatment (red solid line) is red-shifted and a decrease of the reflectance is observable. This shift is probably due to an increase of the thin surface oxide layer, i.e. an increase of material with optical index different from air. In Figure 7(d) the reflectance of the grating modified with the FDPA molecule is shown after modification (solid green line) and before modification (solid black line). Figure 7(e) demonstrates that the reflectance of the grating modified with the EGPA molecule (solid blue line) changes compared to the reflectance before modification (solid black line).

Figure 7(b), which summarizes the reflectance measurement results, allows to discuss the plasmonic peak shape modification by phosphonate adsorption. On top, the FDPA (green line) and the EGPA (blue line) spectra on a flat mirror-like surface are shown. On the bottom, the relative variation of reflectance $\Delta R/R$ obtained for light polarized perpendicular to the grating before and after modification reveals differences depending on the treatment of the grating. The strongest shape modification is observed for the FDPA treated grating. In the spectral range from 1000-1100 cm^{-1} a difference of 3 % in terms of $\Delta R/R$ is found compared to the grating which has received the dummy treatment. This variation of 3 % has to be compared with the value of 0.3 % obtained by the ratio of FDPA and dummy treated mirror surfaces (spectra on top). We report therefore a ten-fold signal enhancement. For molecular absorption lines outside of the spectral region of plasmonic resonance, no enhancement effect is found (see carbon-fluorine vibrations in between 1200-1250 cm^{-1}). The modification of the grating by EGPA is less pronounced than the modification by the FDPA treatment. The main difference of $\Delta R/R$ in between the EGPA and the dummy treatment is the shape modification. While the dummy treatment leads to a dip, the EGPA treatment reveals a zigzag-shape. The physical principle underlying this shape variation will be discussed in the following, but we want to finish this description part by underlining that the phosphonate adsorption on the mid-IR plasmonic gratings lead to $\Delta R/R$ signal variation in the percent range, while phosphonate adsorption on flat mirror-like surface lead to $\Delta R/R$ signal variation in the per mille range.

The described signal enhancement is due to a plasmonic effect and is strongest around the localized surface plasmon resonance, here from 900-1100 cm^{-1}. The principle of surface-plasmon resonance (SPR) sensors is to excite a plasmonic resonance with incident light and to detect a shift of a plasmonic resonance peak upon modifying the optical environment of the resonator by bringing minute quantities of analyte to its surface [36]. The SPR-sensing principle does not require a spectral overlap of plasmonic resonance mode and analyte vibration mode, but when these two modes indeed overlap, then the plasmonic mode leads to surface-enhanced infrared absorption (SEIRA) of the molecules IR-mode [2]. This interaction of radiative plasmonic modes and absorbing molecule vibration modes can be described using a weak-coupling model [37,38]. Gallinet *et. al.* [39] propose a theoretical model to describe the asymmetric modulation of the plasmonic resonance due to an overlap of plasmonic resonance and molecule absorption. The dummy treatment leads most likely to a plasma induced oxide around the plasmonic resonator and this red-shifts the main plasmonic peak. The observable SPR-shift, i.e. the $\Delta R/R$ dip, allows therefore to measure minute quantities of surface oxide. The phosphonate IR-vibration lines which spectrally overlap with the grating's LSPR mode lead to a $\Delta R/R$ zigzag-shape of the resonance peak, thus a signal originating from SPR and SEIRA effects. The coupling of molecular absorption peaks as broad as the plasmonic resonance width which was investigated in this study has to be compared with spectrally sharp molecular absorption peaks coupled to spectrally broad plasmonic resonances. Such experiments were obtained with the same material system [28,40,41] where a clear separation of SPR and SEIRA was demonstrated. These previous works were focusing on physical deposition of molecules, e.g. by spin coating or drop casting. This work and the focus on a wet-chemical process to bring molecules to the grating surface demonstrates that highly Si-doped InAsSb can be used as plasmonic enhanced

sensor platform to (1) study phosphonates adsorption in a first step and to (2) study advanced semiconductor-organic surface reactions, e.g. relevant for pharmaceutical controlling or biomedical science in a next step.

4. CONCLUSION

In this work, we could show phosphonic acids adsorption on oxygen plasma activated GaSb and InAsSb surfaces. The adsorbed molecules are stable upon baking at 120° C, ultrasonic cleaning with organic solvents and storage for several weeks at ambient conditions. The oxygen plasma activation leads to an increase of III-V surface oxides beyond their native oxide thickness as could be shown by X-ray photoelectron spectroscopy. We tested the influence of plasma treatment and immersion time (6 h or 48 h) in phosphonic acid solution, but could not find significant differences in terms of IR-signature of the adsorbed molecules. Two phosphonic acids with different terminal groups, either ethylene glycol or fluorinated carbon-terminated groups were used in this study and we show that their adsorption allows to modify the hydrophobicity of the surfaces and to protect the surfaces by an anti-fouling cover layer. Infrared spectroscopy on IR-mirror structures fabricated by highly doped III-V semiconductor material indicates partial deprotonation (hydrogenophosphonate or phosphonate ions vibration modes) of the adsorbed phosphonic acid and thus phosphonate bonding to the surfaces. Adsorption of phosphonates on an all-semiconductor mid-IR plasmonic grating structure is detected by a shift and by a shape modulation of the plasmonic resonance peak. Compared with molecule adsorption on flat mirror-like layers, a ten-fold signal enhancement is found. These results show that stable functionalization of InAsSb and GaSb surfaces by phosphonates is possible. All-semiconductor enhanced plasmonic sensing in the mid-IR was demonstrated.

Funding

French Investment for the Future program (EquipEx EXTRA, ANR 11-EQPX-0016); French ANR (SUPREME-B, ANR-14-CE26-0015); European Union's Horizon 2020 research and innovation programme (Marie Sklodowska-Curie grant agreement No 641899); Occitanie region.

Acknowledgements

F. Pichot, J.-M. Peiris and J. Lyonnet are acknowledged for technical support at the cleanroom facilities of Université de Montpellier. G. Boissier, J.-M. Aniel and G. Narcy are acknowledged for technical support. Valérie Flaud is acknowledged for scientific discussions and technical support at the XPS facility of the Institute Charles Gerhard Montpellier. Franck Martin and Michel Granier are acknowledged for discussing phosphonic acid chemistry and the presented infrared spectra.

References

1. A. Krier, ed., *Mid-Infrared Semiconductor Optoelectronics*, Springer Series in Optical Sciences No. 118 (Springer, 2006).
2. F. Neubrech, C. Huck, K. Weber, A. Pucci, and H. Giessen, "Surface-Enhanced Infrared Spectroscopy Using Resonant Nanoantennas," Chem. Rev. (2017).
3. V. N'Tsame Guilengui, L. Cerutti, J.-B. Rodriguez, E. Tournié, and T. Taliercio, "Localized surface plasmon resonances in highly doped semiconductors nanostructures," Appl. Phys. Lett. **101**, 161113 (2012).
4. A. Boltasseva and H. A. Atwater, "Low-Loss Plasmonic Metamaterials," Science **331**, 290–291 (2011).
5. Y. Zhong, S. D. Malagari, T. Hamilton, and D. Wasserman, "Review of mid-infrared plasmonic materials," J. Nanophotonics **9**, 093791–093791 (2015).
6. F. Tao and S. L. Bernasek, *Functionalization of Semiconductor Surfaces* (Wiley, 2012).
7. R. J. Hamers, "Immobilization of Biomolecules at Semiconductor Interfaces," in *Functionalization of Semiconductor Surfaces*, F. F. Tao and S. L. Bernasek, eds. (John Wiley & Sons, Inc., 2012), pp. 401–428.
8. C. W. Wilmsen, ed., *Physics and Chemistry of III-V Compound Semiconductor Interfaces* (Springer US, 1985).
9. Y. Mizokawa, O. Komoda, and S. Miyase, "Long-time air oxidation and oxide-substrate reactions on GaSb, GaAs and GaP at room temperature studied by X-ray photoelectron spectroscopy," Thin Solid Films **156**, 127–143 (1988).
10. S. A. Jewett, J. A. Yoder, and A. Ivanisevic, "Surface modifications on InAs decrease indium and arsenic leaching under physiological conditions," Appl. Surf. Sci. **261**, 842–850 (2012).
11. K. Tsunoda, Y. Matsukura, R. Suzuki, and M. Aoki, "Thermal instability of GaSb surface oxide," in B. F. Andresen, G. F. Fulop, C. M. Hanson, J. L. Miller, and P. R. Norton, eds. (2016), p. 98190S.
12. M. Bomers, F. Barho, M. J. Milla-Rodrigo, L. Cerutti, R. Arinero, F. G.-P. Flores, E. Tournié, and T. Taliercio, "Pedestal formation of all-semiconductor gratings through GaSb oxidation for mid-IR plasmonics," J. Phys. Appl. Phys. **51**, 015104 (2018).

13. W. Knoben, S. H. Brongersma, and M. Crego-Calama, "Preparation and Characterization of Octadecanethiol Self-Assembled Monolayers on Indium Arsenide (100)," J. Phys. Chem. C **113**, 18331–18340 (2009).
14. D. Y. Petrovykh, J. C. Smith, T. D. Clark, R. Stine, L. A. Baker, and L. J. Whitman, "Self-Assembled Monolayers of Alkanethiols on InAs," Langmuir **25**, 12185–12194 (2009).
15. A. Shaporenko, K. Adlkofer, L. S. O. Johansson, M. Tanaka, and M. Zharnikov, "Functionalization of GaAs Surfaces with Aromatic Self-Assembled Monolayers: A Synchrotron-Based Spectroscopic Study," Langmuir **19**, 4992–4998 (2003).
16. R. Stine, E. H. Aifer, L. J. Whitman, and D. Y. Petrovykh, "Passivation of GaSb and InAs by pH-activated thioacetamide," Appl. Surf. Sci. **255**, 7121–7125 (2009).
17. Y. A. Wang, J. J. Li, H. Chen, and X. Peng, "Stabilization of Inorganic Nanocrystals by Organic Dendrons," J. Am. Chem. Soc. **124**, 2293–2298 (2002).
18. K. Bastekova, O. Guselnikova, P. Postnikov, R. Elashnikov, M. Kunes, Z. Kolska, V. Švorčík, and O. Lyutakov, "Spatially selective modification of PLLA surface: From hydrophobic to hydrophilic or to repellent," Appl. Surf. Sci. **397**, 226–234 (2017).
19. O. Guselnikova, P. Postnikov, R. Elashnikov, M. Trusova, Y. Kalachyova, M. Libansky, J. Barek, Z. Kolska, V. Švorčík, and O. Lyutakov, "Surface modification of Au and Ag plasmonic thin films via diazonium chemistry: Evaluation of structure and properties," Colloids Surf. Physicochem. Eng. Asp. **516**, 274–285 (2017).
20. A. Keys and A. R. Barron, "Growth of self-assembled monolayers on sulfide treated gallium arsenide using predetermined linkage moieties," Main Group Chem. **4**, 263–271 (2005).
21. R. Artzi, S. S. Daube, H. Cohen, and R. Naaman, "Adsorption of Organic Phosphate as a Means To Bind Biological Molecules to GaAs Surfaces," Langmuir **19**, 7392–7398 (2003).
22. A. M. Botelho do Rego, A. M. Ferraria, J. El Beghdadi, F. Debontridder, P. Brogueira, R. Naaman, and M. Rei Vilar, "Adsorption of phenylphosphonic acid on GaAs (100) surfaces," Langmuir **21**, 8765–8773 (2005).
23. S. P. Pujari, L. Scheres, A. T. M. Marcelis, and H. Zuilhof, "Covalent Surface Modification of Oxide Surfaces," Angew. Chem. Int. Ed. **53**, 6322–6356 (2014).
24. G. Guerrero, J. G. Alauzun, M. Granier, D. Laurencin, and P. H. Mutin, "Phosphonate coupling molecules for the control of surface/interface properties and the synthesis of nanomaterials," Dalton Trans. **42**, 12569 (2013).
25. J. B. Brzoska, I. B. Azouz, and F. Rondelez, "Silanization of solid substrates: a step toward reproducibility," Langmuir **10**, 4367–4373 (1994).
26. W. Gao, L. Dickinson, C. Grozinger, F. G. Morin, and L. Reven, "Order- Disorder Transitions in Self-Assembled Monolayers: A 13C Solid-State NMR Study," Langmuir **13**, 115–118 (1997).
27. T. Taliercio, V. N. Guilengui, L. Cerutti, E. Tournié, and J.-J. Greffet, "Brewster "mode" in highly doped semiconductor layers: an all-optical technique to monitor doping concentration," Opt. Express **22**, 24294 (2014).
28. F. B. Barho, F. Gonzalez-Posada, M.-J. Milla-Rodrigo, M. Bomers, L. Cerutti, and T. Taliercio, "All-semiconductor plasmonic gratings for biosensing applications in the mid-infrared spectral range," Opt. Express **24**, 16175 (2016).
29. Y. Yuan and T. R. Lee, "Contact Angle and Wetting Properties," in *Surface Science Techniques*, G. Bracco and B. Holst, eds. (Springer Berlin Heidelberg, 2013), Vol. 51, pp. 3–34.
30. S. A. Paniagua, P. J. Hotchkiss, S. C. Jones, S. R. Marder, A. Mudalige, F. S. Marrikar, J. E. Pemberton, and N. R. Armstrong, "Phosphonic Acid Modification of Indium−Tin Oxide Electrodes: Combined XPS/UPS/Contact Angle Studies †," J. Phys. Chem. C **112**, 7809–7817 (2008).
31. P. Harder, M. Grunze, R. Dahint, G. M. Whitesides, and P. E. Laibinis, "Molecular conformation in oligo (ethylene glycol)-terminated self-assembled monolayers on gold and silver surfaces determines their ability to resist protein adsorption," J. Phys. Chem. B **102**, 426–436 (1998).
32. D. Seo, J. Na, S. Lee, and S. Lim, "Behavior of GaSb (100) and InSb (100) surfaces in the presence of H2O2 in acidic and basic cleaning solutions," Appl. Surf. Sci. **399**, 523–534 (2017).
33. G. Hollinger, R. Skheyta-Kabbani, and M. Gendry, "Oxides on GaAs and InAs surfaces: An x-ray-photoelectron-spectroscopy study of reference compounds and thin oxide layers," Phys. Rev. B **49**, 11159 (1994).
34. D. M. Spori, N. V. Venkataraman, S. G. P. Tosatti, F. Durmaz, N. D. Spencer, and S. Zürcher, "Influence of Alkyl Chain Length on Phosphate Self-Assembled Monolayers," Langmuir **23**, 8053–8060 (2007).
35. L. Portilla and M. Halik, "Smoothly Tunable Surface Properties of Aluminum Oxide Core–Shell Nanoparticles By A Mixed-Ligand Approach," ACS Appl. Mater. Interfaces **6**, 5977–5982 (2014).
36. J. Homola, ed., *Surface Plasmon Resonance Based Sensors*, Springer Series on Chemical Sensors and Biosensors (Springer Berlin Heidelberg, 2006), Vol. 4.
37. S. Kalusniak, S. Sadofev, and F. Henneberger, "Resonant interaction of molecular vibrations and surface plasmon polaritons: The weak coupling regime," Phys. Rev. B **90**, 125423 (2014).
38. R. Adato, S. Aksu, and H. Altug, "Engineering mid-infrared nanoantennas for surface enhanced infrared absorption spectroscopy," Mater. Today **18**, 436–446 (2015).
39. B. Gallinet, T. Siegfried, H. Sigg, P. Nordlander, and O. J. F. Martin, "Plasmonic Radiance: Probing Structure at the Ångström Scale with Visible Light," Nano Lett. **13**, 497–503 (2013).
40. M. J. Milla, F. Barho, F. González-Posada, L. Cerutti, B. Charlot, M. Bomers, F. Neubrech, E. Tournie, and T. Taliercio, "Surface-enhanced infrared absorption with Si-doped InAsSb/GaSb nano-antennas," Opt. Express **25**, 26651–26661 (2017).
41. F. B. Barho, F. Gonzalez-Posada, M.-J. Milla, M. Bomers, L. Cerutti, E. Tournié, and T. Taliercio, "Highly doped semiconductor plasmonic nanoantenna arrays for polarization selective broadband surface-enhanced infrared absorption spectroscopy of vanillin," Nanophotonics **7**, (2017).